Experimental and numerical analysis of textile composite draping on a square box. Influence of the weave pattern

J. Huang, P. Boisse, N. Hamila, I. Gnaba, D. Soulat, Peng Wang

Version of Record: https://www.sciencedirect.com/science/article/pii/S0263822321003056
Manuscript_ede6ccb8f2058f9c97cdff4c7fe76c2c

Experimental and numerical analysis of textile composite draping on a square box. Influence of the weave pattern

J. Huang[a], P. Boisse[a*], N. Hamila[d], I. Gnaba[b], D. Soulat[b], P. Wang[c]

[a]*Université de Lyon, LaMCoS CNRS, INSA Lyon, F-69621 France*
[b]*Université de Lille, ENSAIT, GEMTEX, F-59000, Roubaix, France*
[c]*Université de Haute Alsace, ENSISA, LPMT, F-68000 Mulhouse, France*
[d]*ENI Brest, IRDL CNRS, F-29200 Brest, France*

Abstract

Draping of composite textile reinforcements on a square box was analyzed experimentally and by numerical simulation. This forming is difficult for fabrics with continuous fibers due to the quasi inextensibility of the fibers. It is shown that the feasibility of draping on a square box with a large depth depends on the weave pattern of the textile reinforcement. Simultaneous forming of several plies without defects is also obtained. A simulation approach based on stress resultant shell finite elements gives results in agreement with the experiments, in particular with regard to the development (or not) of wrinkling. This numerical simulations show that the characteristics of tension, in-plane shear and bending of the textile reinforcement take into account the type of weave pattern and have a major role to play in the feasibility of draping. In particular, it is shown that the ratio of in-plane shear stiffness to bending stiffness of a satin weave reinforcement is favorable for draping it over a square box without wrinkling.

Keywords: Draping, Square box, Textile composite reinforcements, Weaving pattern, Mechanical properties, Wrinkling.

1. Introduction

The forming of textile reinforcements is often necessary to produce composite parts of complex geometry, generally with double curvatures. This forming, often called draping,

*Corresponding author.
E-mail address: philippe.boisse@insa-lyon.fr (P. Boisse).

concerns dry reinforcements (without a matrix) in Liquid Composite Molding (LCM) processes [1-5], thermoset prepregs [6-9] or thermoplastic prepregs [9-14]. Although these processes are different, the forming operation is driven by the textile reinforcement. The mechanical behavior of textile reinforcements during the forming process is very specific due to their fibrous composition, which makes relative slippage of the fibers possible but forces the fibers to be almost inextensible. Consequently, the draping processes are often challenging. The parameters that condition the forming process of a given shape are numerous and include the nature of the textile reinforcement, the efforts on the tools, friction and the manufacturing speed. Numerical simulation of the draping process is an important tool as it makes it possible to determine the feasibility of draping and the optimum parameters and thus avoid costly development of the process through trial and error.

For the analysis of processes, materials, constitutive laws and simulation approaches, different geometries that constitute test cases or benchmarks are considered. Among them, the square box or square cup is a classic shape and corresponds to some industrial parts. It is much used as a test case for ductile metals that can be formed on this geometry thanks to possible axial strains. This geometry was taken as a benchmark at the NUMISHEET 1993 conference and is commonly used for metal forming analysis [15, 16].

When draping textile composite reinforcements, the modes of deformation during forming are different. The fibers are nearly inextensible and the membrane deformations that are necessary to obtain double curved geometries are mainly in-plane shear strains corresponding to angle changes between warp and weft directions. The hemispherical shape is widely used as a test for the analysis of the draping of woven composite reinforcements [17-22] and the forming of non-crimp fabrics [23-26]. The forming on this shape gives rise to significant in-plane shear, but can be performed without defect for a large part of the textile reinforcements when blank holders are used [27]. Other geometries are also used to analyze the draping of

textile reinforcements of composites. The double dome has been proposed as a forming benchmark [28-32]. The tetrahedral shape is interesting because it corresponds to case corner parts [33-36].

Although the square box is a basic geometry which is used for the analysis of deep drawing of metallic materials, limited knowledge exists about the forming of textile reinforcements with continuous fibers on a this shape. Publications and results are rare both from an experimental and simulation point of view. Draping on a square box is sometimes considered impossible when the stamping depth is large. The few forming experiments on a square box presented in articles result in significant wrinkling in the corners of the square box [37,38]. Bae et al. analysed the thermoforming of carbon fiber/epoxy prepregs with a square-cup geometry [39]. They achieved a satisfactory forming for a depth/width ratio equal to 0.2, but a ratio equal to 0.4 leads to significant wrinkling and shrinkage. Some simulations of square box forming have been proposed, but they show wrinkles after forming and are not compared to experiments [20, 40].

The objective of this article is to analyze and understand draping of textile reinforcements on a square box with a significant depth (Fig. 1). This draping is difficult, but wrinkling-free stamping are achieved are obtained under certain conditions and in particular for some weave patterns. These formings are carried out for a single ply or for stacks of plies of different orientations. The objective is also to show that the deformation of the textile reinforcement and in particular the onset and development of wrinkling can be predicted by a simulation approach based on stress resultant shells. These simulations make it possible to highlight the reasons for the onset of wrinkling or not. They are based on the behavior of tension, in-plane shear and bending of the textile reinforcement. It is shown that these behaviors are relevant to take into account the influence of the weave pattern which leads to draping with or without wrinkling.

Although the wrinkle development is a global problem which requires a simulation taking into account all the parameters, this study showed that the ratios between the different stiffnesses have an important role in the formation of wrinkles, in particular the ratio between in-plane shear stiffness and bending stiffness.

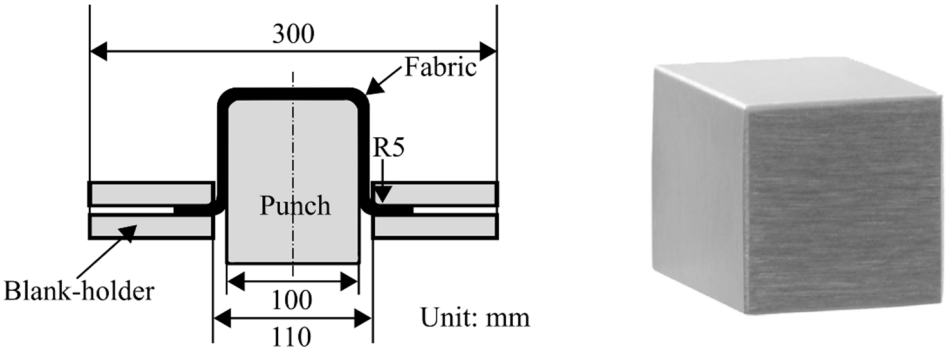

Fig. 1. Geometry of the tools for the square box forming.

2. Mechanical properties of composite reinforcements.

2.1. Presentation of the two studied textile reinforcements

Two textile reinforcements were considered. Fig. 2a displays a glass plain weave and Fig. 2b presents a carbon 5 harness satin. The geometrical characteristics and the areal densities are given in Table 1.

Table 1. Properties of the two textile fabrics.

Type of fabric	Plain weave	5 harness satin
Manufacturer	Hexcel	Hexcel
Thickness (mm)	0.12	0.3
Fiber type	Glass	Carbon
	(EC 968)	(HexTow IM7 GP 6 K)
Number of fibers per yarn	1000	6000
Areal density (g/m^2)	160	290
Number of warp yarns per cm	11.8	6.5
Number of weft yarns per cm	10.7	6.5
Mass distribution of warp yarns (%)	52	50

Mass distribution of weft yarns (%)	48	50

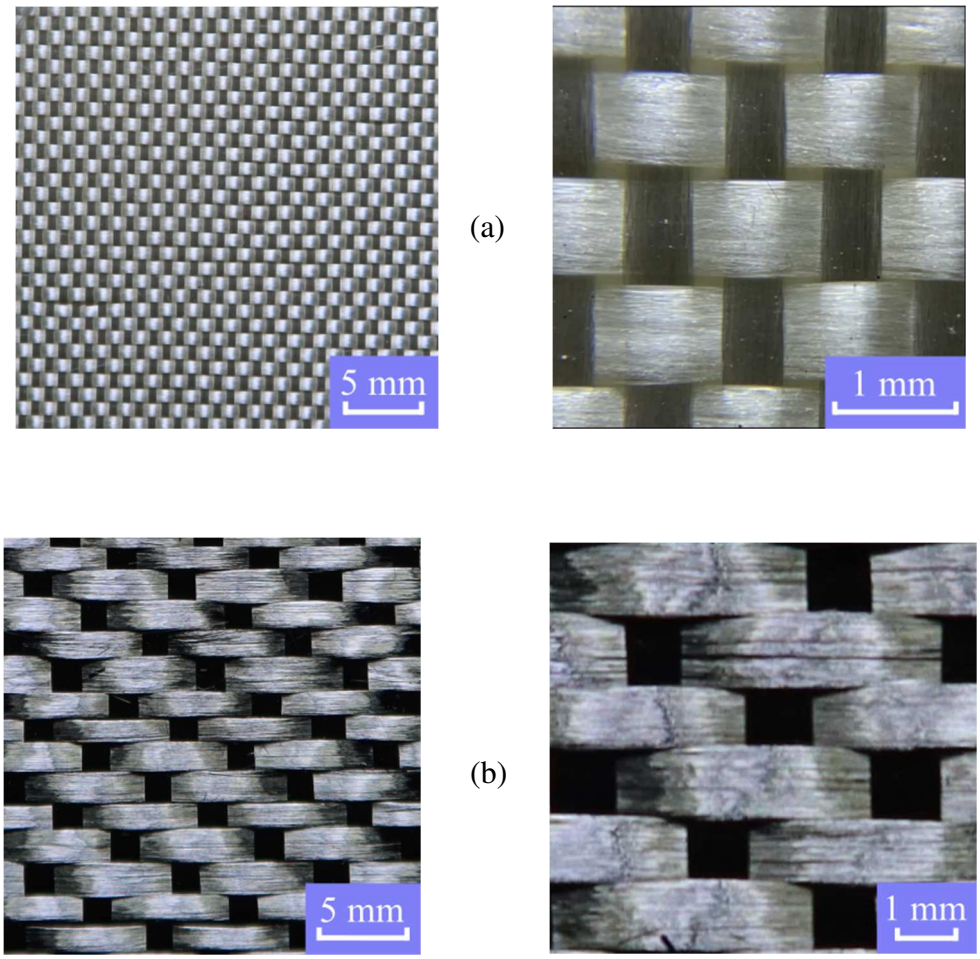

Fig. 2. (a) Glass plain weave. (b) Carbon 5 harness satin.

2.2. Stress resultant shell approach for textile reinforcements

Given the small or moderate thickness of the textile reinforcements, a shell approach is used to simulate the draping of the textile reinforcement and more specifically a stress resultant shell approach specific to woven fabrics [41]. The tensions T^{11} and T^{22} in the warp and weft yarns, the in-plane shear moment C_γ and the bending moments M^{11} and M^{22} are stress resultants on a woven unit cell (Fig. 3) and represent the stress field in the textile reinforcement.

Within the framework of a dynamic approach, the virtual work theorem can, for any virtual displacement, be written on the boundary with prescribed displacements:

$$\delta W_{ext} - \delta W_{int} - \delta W_{acc} = 0 \tag{1}$$

Here, $\delta W_{ext}, \delta W_{int}, \delta W_{acc}$, are the virtual works of external, internal and acceleration quantities.

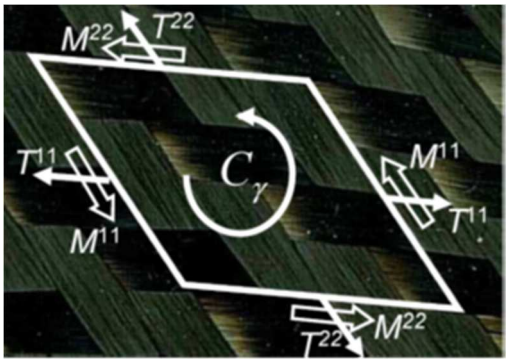

Fig. 3. Stress resultants on a unit cell.

In stress resultant shell approaches for textile reinforcement, the virtual internal work is composed of the works of tension δW_t, in-plane shear δW_s, and bending δW_b and takes the following form [41]:

$$\delta W_{\text{int}} = \delta W_t + \delta W_s + \delta W_b = \underbrace{\sum_{P=1}^{ncell} {}^P\delta\varepsilon_{11}\,{}^P T^{11}\,{}^P L_1 + {}^P\delta\varepsilon_{22}\,{}^P T^{22}\,{}^P L_2}_{\text{Tension}} + \underbrace{\sum_{P=1}^{ncell} {}^P\delta\gamma\,{}^P C_\gamma}_{\text{In plane shear}} + \underbrace{\sum_{P=1}^{ncell} {}^P\delta\chi_{11}\,{}^P M^{11}\,{}^P L_1 + {}^P\delta\chi_{22}\,{}^P M^{22}\,{}^P L_2}_{\text{Bending}} \tag{2}$$

In Eq. (2), ${}^pA$ is the quantity A for the woven unit cell number p, *ncell* is the number of woven cells in the textile reinforcement, $\delta\varepsilon_{11}$ and $\delta\varepsilon_{22}$ are respectively the virtual axial strains in the warp and weft directions, $\delta\gamma$ is the virtual in-plane shear angle and $\delta\chi_{11}$ and $\delta\chi_{22}$ are the virtual bending curvatures in the warp and weft directions. The mechanical behavior of the textile reinforcement is given by the tensions T^{11} and T^{22} as a function of the axial strains ε_{11} and ε_{22},

the in-plane shear moment C_γ as a function of the in-plane shear angle γ and the bending moments M^{11} and M^{22} as a function of the curvatures χ_{11} and χ_{22}.

Eq. (2) is a shell approach based on the stress resultants T^{11} and T^{22}, C_γ, M^{11} and M^{22}. It is a simplified approach and, in addition, the coupling between the stiffness of different deformation modes are not taken into account. Although some works have shown that couplings exist, [42-46], the choice was made not to consider them in this study for reasons of simplicity but also because of the difficulty in obtaining experimental data. The approach given in Eq. (2) involves the bending behavior of the textile reinforcement. Simulations of the draping of textile reinforcements based on membrane approaches (no bending stiffness) have been developed [19, 23, 32, 47-49]. However, it has been shown that accounting for the bending stiffness is highly important for the simulation of wrinkling [36, 50-55]. To perform a draping simulation based on Eq. (2), it is necessary to know the tension, plane shear and bending behaviors of the textile reinforcement. As in most shell theories, compaction strains in the thickness are not considered. To analyze the mechanical behavior through the thickness, it would be necessary to carry out simulations based on 3D elements [35, 56-58] or solid-shell elements [59, 60]. A shell approach is relevant for the analysis of the draping on a square box.

2.3. Mechanical characteristics of textile reinforcements.

2.3.1. In-plane shear properties

In-plane shear properties of the two studied woven fabrics were obtained by a bias extension test (Fig. 4). This test and the picture frame test were the two main experiments for the analysis of the behavior of textile reinforcements in plane shear. They have given rise to numerous researches [61-68].

Fig. 4a shows the geometry of the bias extension test specimen. The yarns of the fabric were oriented at ±45° from the tensile direction. The specimen was subjected to in-plane shear and

three constant shear zones developed. The shear angle in the central area of the specimen could be measured by optical measurements or deduced from the elongation of the specimen by assuming the yarns were inextensible.

The shear moment C_γ in Eq. (2) is related to the tensile force F on the specimen measured for a shear angle γ by stating the equality of the powers developed by the test machine and by the shear of the specimen [64, 65].

$$C_\gamma(\gamma) = \frac{F\,D}{\ell(2D-\ell)}\left(\cos\frac{\gamma}{2} - \sin\frac{\gamma}{2}\right) - \frac{\ell}{2D-\ell}C_s\left(\frac{\gamma}{2}\right) \tag{3}$$

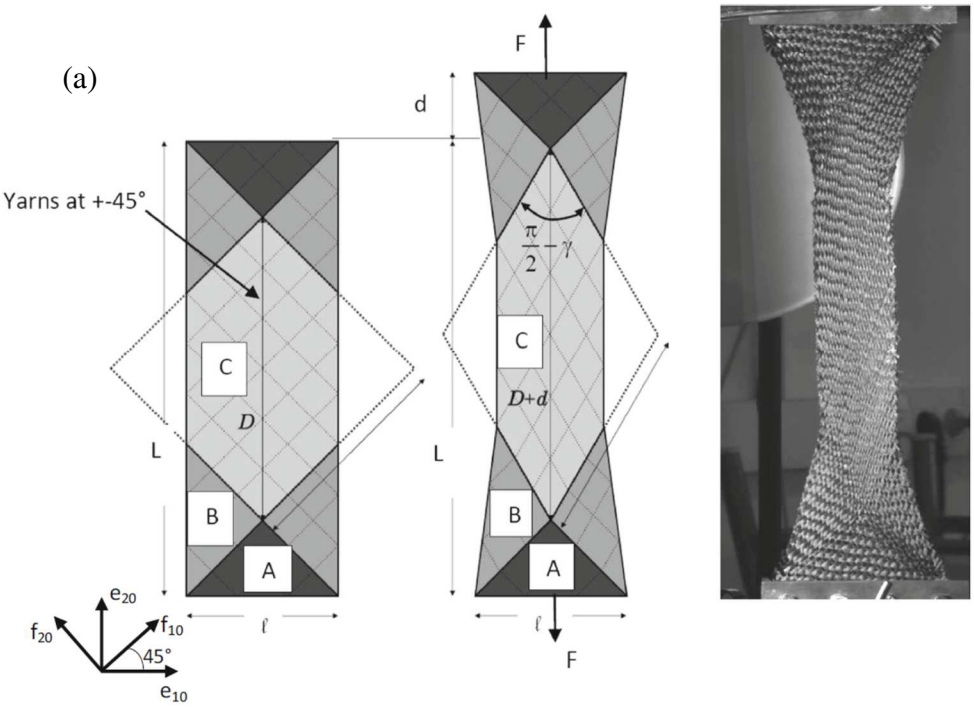

(b)

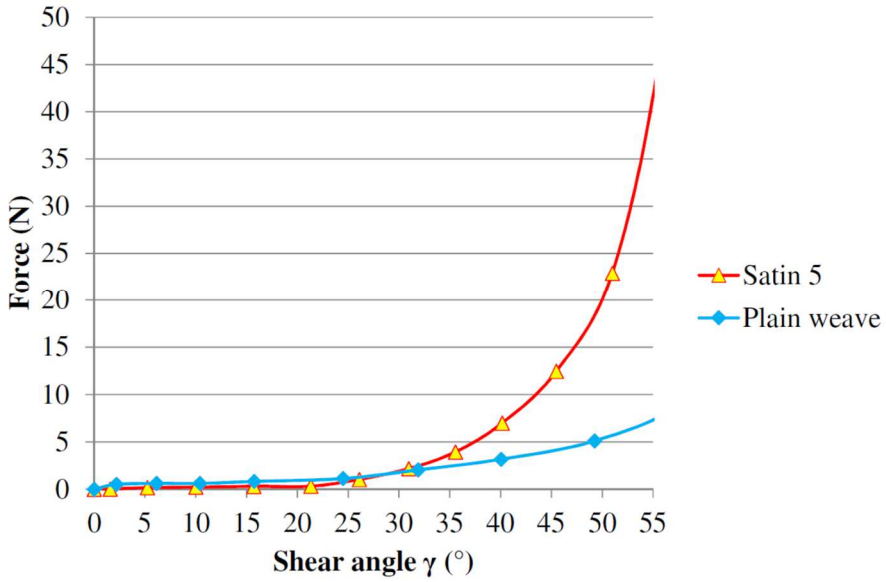

Fig. 4. (a) Bias extension test. (b) Force versus shear angle for the two fabrics.

Dimensions D and ℓ are defined in Fig. 4a. Since it is simple to implement, this bias extension test is frequently used. The curves Fig. 4b show that, although its density is significantly lower, the shear stiffness of glass plain weave is slightly higher than that of carbon satin weave for angles smaller than 25° (although the glass plain weave is only a third of the thickness). For larger angles, the carbon satin is stiffer. The in-plane shear properties used in the simulations carried out in sections 4 to 6 are given in Table 2.

Table 2. In-plane shear properties of the two fabrics.

Materials	In-plane shear moment (N mm)
	$C_\gamma(\gamma) = K_1\gamma + K_2\gamma^3 + K_3\gamma^5$
Plain weave E-Glass	$K_1 = 1.66\times10^{-2}\pm6\times10^{-4}$, $K_2 = 1.46\times10^{-2}\pm7\times10^{-4}$,
	$K_3 = -4.19\times10^{-3}\pm5.6\times10^{-4}$
Carbon 5 harness satin	$K_1 = 6.44\times10^{-4}\pm5.6\times10^{-5}$, $K_2 = 5.95\times10^{-2}\pm5.9\times10^{-3}$,
	$K_3 = 1.07\times10^{-1}\pm1.5\times10^{-2}$

2.3.2. Bending properties

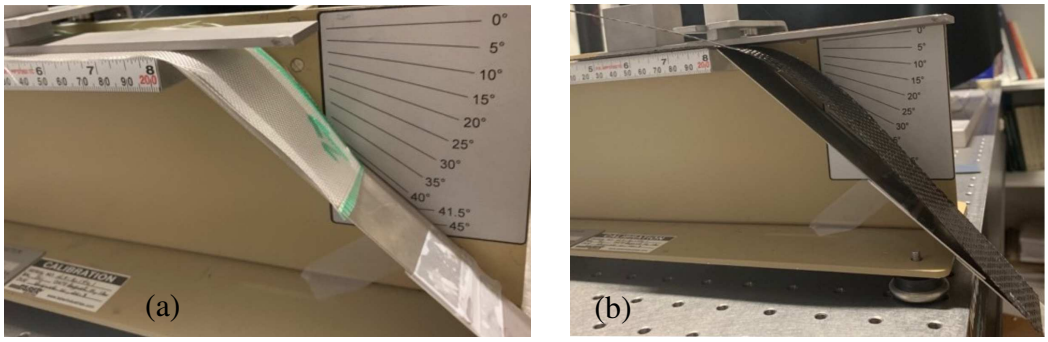

Fig. 5. Cantilever bending test. (a) Glass plain weave. (b) Carbon 5 harness satin weave.

The cantilever bending test initiated by Pierce [69] is performed by subjecting a specimen to its own weight [54, 70-72]. Although viscoelastic models of bending behavior have been proposed for fibrous reinforcement bending [73-76], it is assumed here that the bending behavior is elastic. Fig. 5 shows this bending test in the case of the glass plain weave and carbon satin weave. A simple way to analyze the test is to advance the specimen until it touches a plane inclined at 41.5° and measure the distance ℓ along this plane. Assuming a linear relationship between the bending moment M and the curvature χ, and denoting w the weight per unit length of the specimen, the bending behavior is given by [69]:

$$M = G\chi \qquad G = \frac{\ell^3}{8} w \tag{4}$$

The bending properties of the two fabrics are given in Table 3. The satin weave was much stiffer in bending than the plain weave.

Table 3. Bending stiffness of the two fabrics.

Materials	Bending stiffness G (N·mm)
Plain weave E-Glass	0.102 ± 0.016
Carbon 5 harness satin	3.42 ± 0.44

2.3.3. Tensile properties

The tension stiffnesses of the woven fabrics are large. The behavior is biaxial since the extensions of the fabric in the warp and weft directions were coupled by the weave [77-80]. However, for the sake of simplicity, the tensile behavior was assumed to be linear and decoupled (Table 4).

Table 4. Tensile stiffness of the two fabrics.

Materials	Tensile stiffness (N/mm)
Plain weave E-Glass	1440
Carbon 5 harness satin	29300

3. Square box draping experiments

(a)  (b) 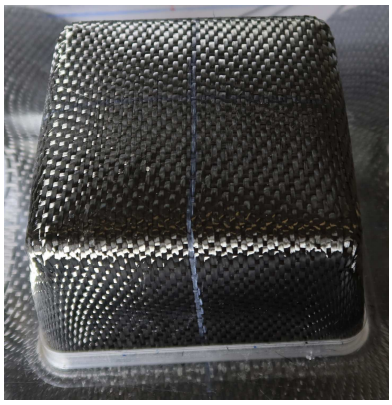

Fig. 6. Square box forming of a single ply oriented at 0-90°.
(a) Glass plain weave. (b) Carbon satin weave.

The square box forming process, whose tool geometry is shown in Fig. 1., was carried out for both fabrics. The blank holder put a 0.05-MPa pressure on the exterior part of the fabric and the punch moved 75mm at a speed of 45 mm/min. The depth/width ratio is 0.75. The shaping was carried out for a 0-90° orientation (Fig. 6) (yarns parallel to the edges of the square box) and a ±45° orientation (Fig. 7).

(a)  (b) 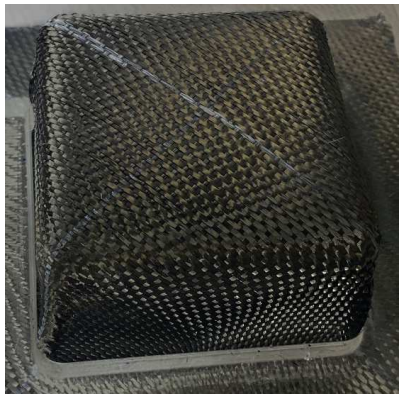

Fig. 7. Square box forming of a single ply oriented at ±45°.
(a) Glass plain weave. (b) Carbon satin.

Experimental results of the square box forming are shown in Figs. 6a and 7a for the glass plain weave and in Figs. 6b and 7b for the carbon satin. It can be seen that the forming of the satin weave was possible without wrinkling of the reinforcement in this case with a significant depth/width ratio of 0.75. Conversely, the forming of the glass plain weave on the square box led to a significant amount of wrinkles. The square box shape could not be reached with this plain weave reinforcement. These experiments demonstrate that the weaving pattern of textile reinforcement strongly conditioned the possibility of draping.

Some publications claim that satin weave leads to good drapability [81] without this quantity being clearly defined and quantified. In [61, 62, 66, 82-84], the possibility to carry out a forming is related to the in-plane shear characteristics and the locking angle. It will be seen in the following that this is not sufficient and that, in particular, the bending characteristics play an important role.

4. Simulation of the square box forming

4.1. Stress resultant shell finite elements

Based on the virtual work theorem (Eqs. (1) and (2)), a stress resultant shell element has been developed in Hamila et al. [41] and was used in the present work. The element is composed of elementary woven cells (Fig. 3) and is rotation free, i.e. without any degree of freedom in rotation. It uses the position of the nodes of the neighboring elements to determine the curvatures and the internal bending forces [85]. The expressions of the nodal tensile, shear and bending loads are briefly presented in Appendix A.

4.2 Simulation of the square box forming

The draping processes on a square box presented in Figs. 6 and 7 were simulated using the stress resultant shell finite elements and the mechanical characteristics of the two textile reinforcements identified in section 2.3.

(a) (b)

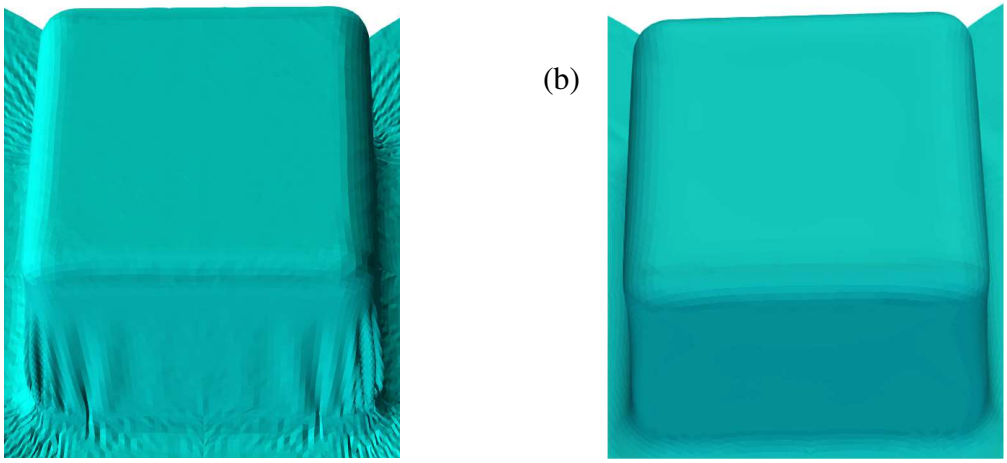

Fig. 8. Simulation of a square box forming.
(a) Glass plain weave and (b) carbon satin weave, oriented at 0-90°

Simulation results of the square box forming (Figs. 8 and 9) were consistent with the experiments. Simulations of the draping of the satin weave reinforcement led well to forming without wrinkling for both orientations whereas the simulations of the forming of glass plain weave led to important wrinkles. Fig. 10 show the large shear angles obtained by the simulation of the forming of the carbon satin weave for a 50 mm displacement of the punch.

(a) (b)

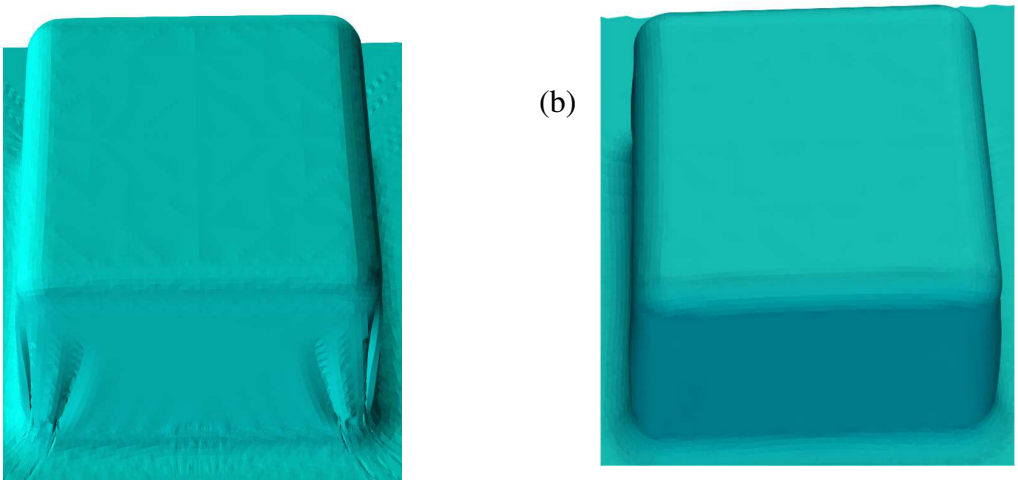

Fig. 9. Simulation of a square box forming.

(a) Glass plain weave and (b) carbon satin weave, oriented at ±45°

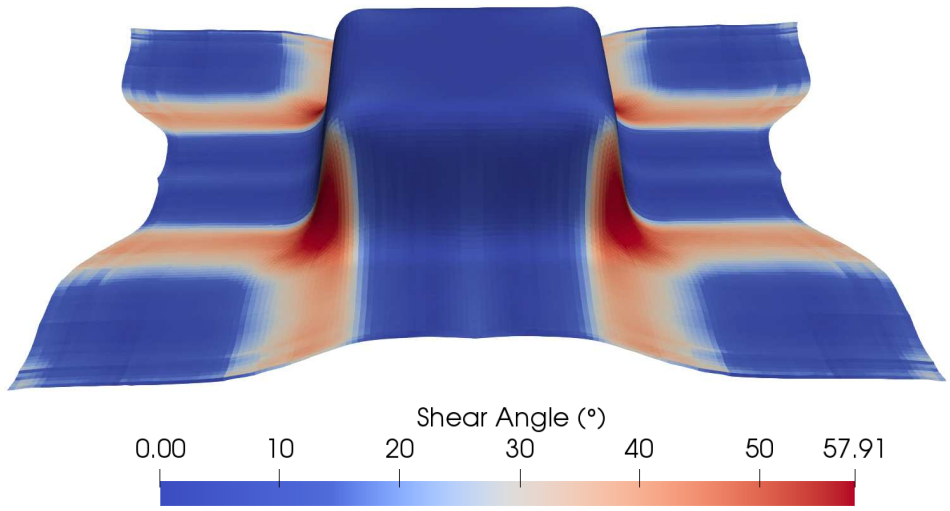

Fig. 10. Shear angles in the simulation of the forming of a carbon satin weave on a square box.

5.3. Importance of the weave pattern.

The great difference in drapability of the two studied woven fabrics is linked to their weave pattern which determines the internal geometry of the fabric and influences their mechanical characteristics. These mechanical properties taken into account in the global dynamic equation during forming (Eqs. (1) and (2)) lead to a deformation of the textile reinforcement in its plane or to an out-of-plane displacement i.e. wrinkling. This depends on all process parameters (geometry, boundary conditions, and material characteristics). Among these characteristics, the bending stiffness decreases the tendency to wrinkling while the in-plane shear stiffness increases it. A high ratio of in-plane shear stiffness to bending stiffness increases the tendency to wrinkling. The weave pattern of the textile reinforcement conditions its internal architecture and defines this ratio. For the two textile reinforcements studied, it is significantly lower in the case of satin weave because its bending rigidity is high. In a similar way, a thick 3D composite reinforcement with high bending stiffness has shown its ability to be formed without wrinkling on complex double-curved shapes such as tetrahedral without blank holder [86, 87].

Furthermore, it is not possible to conclude whether or not wrinkling develops only from the shear locking angle (i.e., the shear angle at which wrinkles are assumed to develop) as proposed in some studies [61, 62, 66, 82-84]. The shear angle obtained on the vertical edges of the square box with the satin weave was 69° (experimental) and 67° (numerical). These angle are greater than the shear locking angle of the satin weave. They are obtained without wrinkling because of the tensions imposed by the forming process.

The type of fiber (glass or carbon) is not an essential issue. Fig. 11 shows the square box forming for a carbon plain weave [37]. The properties of this carbon plain weave fabric are given in Table 5. Very severe wrinkles made draping impossible.

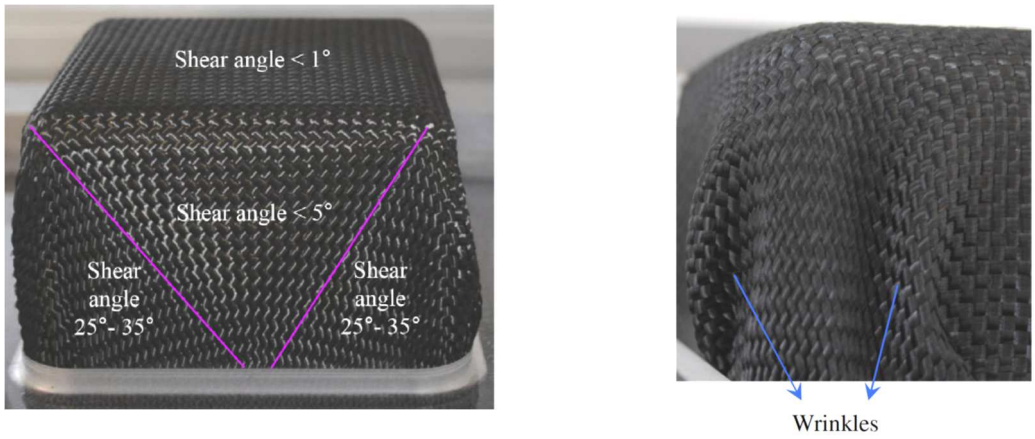

Fig. 11. Square box forming of a carbon plain weave.

Table 5. Properties of the carbon plain weave.

Type of fabric	Plain weave
Manufacturer	Toho-Tenax
Thickness (mm)	0.1
Fiber type	Carbon
Number of filaments per yarn	12000
Areal density(g/m^2)	500
Number of warp yarns per cm	5
Number of weft yarns per cm	5
Mass distribution of warp yarns (%)	50

Mass distribution of weft yarns (%)	50

5. Simultaneous forming of four plies with different fiber orientations

The square box forming of a stack with four layers with different orientation is carried out experimentally (Fig. 12). Such draping process is known to be difficult. Indeed the displacements and deformations of the differently oriented layers are not the same due to the inextensibility of the fibers which takes place in different directions [19, 88-90]. Substantial slippage between the plies occur and wrinkles were frequently observed. Experimental analysis and simulation are presented here only for the satin weave reinforcement. The draping of the plain weave reinforcement which led to significant wrinkling for one layer (Figs. 6a and 7a) is not possible for several layers of different orientations.

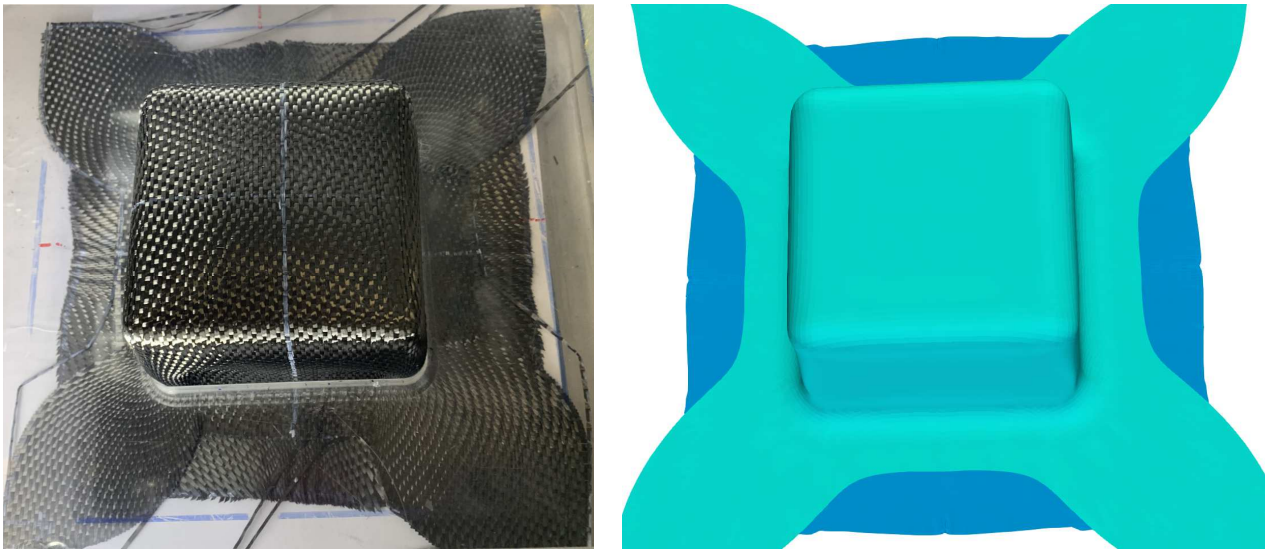

(a) (b)

Fig. 12. Square box forming of four plies $[0°/90°, -45°/45°]_2$. (a) Experiment. (b) Simulation.

Fig. 12 displays the result of the experimental forming and the corresponding simulation. It can be seen that the forming of the four plies of satin weave with different orientation it gives a satisfactory result without wrinkling. This is well achieved by the simulation. In these

multilayer drapings, the differing orientation of the plies leads to significant slippage between the layers, which can be clearly seen in Fig. 12.

6. Experiments and simulations of hemispherical formings.

This article mainly concerns the forming of textile reinforcements on a square box. However, it is interesting to see if the conclusions obtained for the square box, in particular the influence of the weave pattern, are also valid for a classical shape such as the hemisphere. The hemisphere is a simple shape but clearly double curved and requires large in-plane shear deformations to be achieved.

Fig. 13. Hemispherical forming of plain weave and satin weave textile reinforcements.

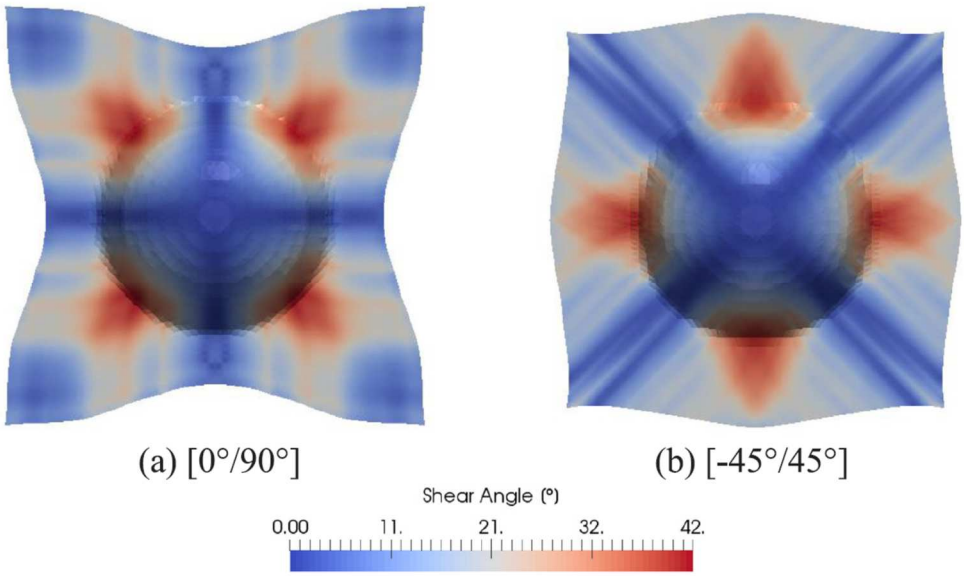

Fig. 14. Simulation of a single ply hemispherical forming.

Both plain weave and satin weave single layers are formed without wrinkling (Fig. 13) [91]. The simulations are in good agreement with experiments both in terms of the absence of wrinkles and the values of the shear angles (Fig. 14). The deformations obtained for the two reinforcements are almost identical.

Forming four plies with different orientations leads to wrinkling in the case of plane weave fabric Fig. 15a. On the contrary, Fig. 15b illustrates that the simultaneous forming of four carbon satin plies could be done wrinkle-free. This example confirms the greater drapability of carbon satin weave. The simulations are in good agreement and show the wrinkling for plain weave and their absence in the case of satin weave (Fig. 16).

(a) (b)

Fig. 15. Hemispherical forming of four plies $[0°/90°, -45°/45°]_2$.
(a) Glass plain weave. (b) Carbon satin weave.

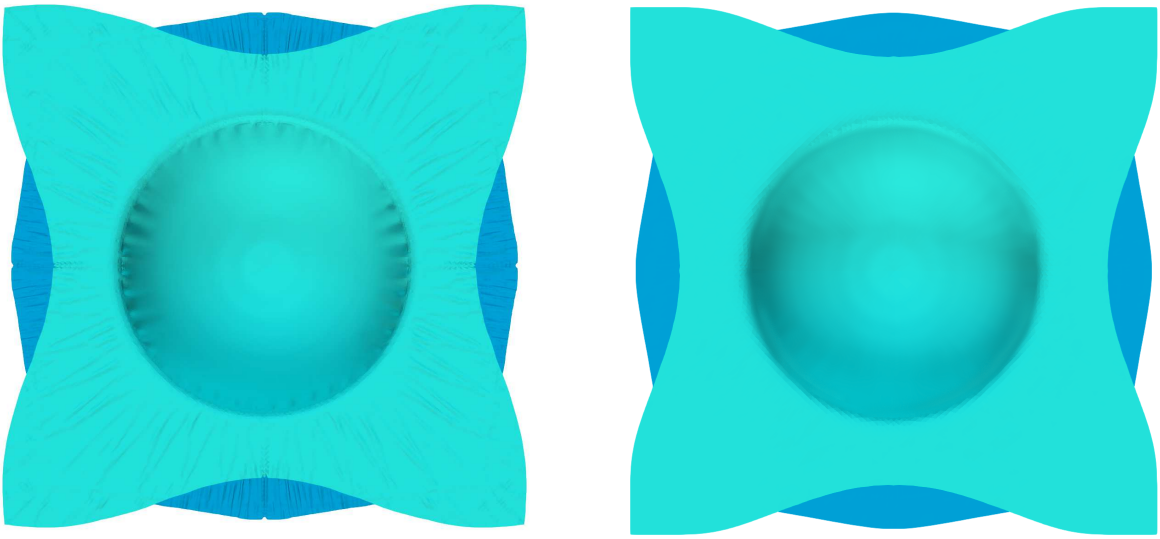

(a) (b)

Fig. 16. Simulation of the hemispherical forming of four plies $[0°/90°, -45°/45°]_2$.
(a) Glass plain weave. (b) Carbon satin weave.

In brief, while it is possible to form a single plain weave ply on a hemisphere, draping remains more difficult for the plain weave, which leads to wrinkles when forming four plies of different orientation. Satin weave, on the other hand, makes it possible to form such shapes without defects. Simulations predict in a relevant way whether or not wrinkling will occur.

7. Conclusion

Draping textile reinforcements with continuous fibers on a square box with a large depth is difficult and often leads to wrinkling. In the present work, in the case of one and several satin weave plies, draping processes on a square box was carried out without wrinkling. The weaving pattern of the satin fabric leads to mechanical characteristics with a low in-plane shear stiffness/bending stiffness ratio. A high in-plane shear stiffness favours the development of wrinkles, whereas a high bending stiffness tends to keep the fabric in its plane and avoid wrinkling. It has been shown that modelling based on stress resultant shells makes it possible to simulate drapings on a square box and to predict the development or not of wrinkling in agreement with experiments.

The study presented concerns two textile reinforcements. It will be necessary to carry out draping on square boxes with textile reinforcements with different weave patterns and to check if the in-plane shear stiffness/bending stiffness ratio is indeed determining in the development of the wrinkling. The onset and development of wrinkling during forming is a global problem that depends on geometry, boundary conditions and material characteristics. Predicting the wrinkling requires an overall simulation of the process. Nevertheless, for all other things being equal, the in-plane shear stiffness/bending stiffness ratio can be an indicator of the drapability of the textile reinforcement.

Declaration of Competing Interest

The authors report no declarations of interest.

Acknowledgment

This work was supported by Agence Nationale de la Recherche,

grant N° ANR-16-CE08-0042-02 COMP3DRE.

Appendix A. Nodal internal loads of the stress resultant shell element

The three-node shell element based on Eq. (2) uses standard linear interpolation functions. The material coordinates r^1 and r^2 are defined along the warp and weft yarns. From these coordinates, the material vectors $\underline{k}_1$ and $\underline{k}_2$ are defined:

$$\underline{k}_1 = \frac{\partial \underline{x}}{\partial r^1} \quad \underline{k}_2 = \frac{\partial \underline{x}}{\partial r^2} \tag{A1}$$

The elementary nodal loads respectively of tension, in plane shear and bending, are defined by the virtual works of tension, in-plane shear and bending in the element $\delta W_t^e, \delta W_s^e, \delta W_b^e$:

$$\delta W_t^e = \delta u^{eT} F_t^e \quad \delta W_s^e = \delta u^{eT} F_s^e \quad \delta W_b^e = \delta u^{eT} F_b^e \tag{A2}$$

Here, δu^e is the virtual nodal displacement. Given the form of $\delta W_t, dW_s, dW_b$ in Eq. (2), the components of the nodal interior loads are:

Tension: $\left(F_t^e\right)_{ij} = ncelle\left(B_{1ij}T^{11}\frac{L_1}{\left\|\underline{k}_1\right\|^2} + B_{2ij}T^{22}\frac{L_2}{\left\|\underline{k}_2\right\|^2}\right)$ (A3)

In-plane shear: $\left(F_s^e\right)_{ij} = ncelle\ B_{\gamma ij}M^s(\gamma)$ (A4)

Bending: $\left(F_b^e\right)_{km} = ncelle\left(Bb_{1km}M^{11}\frac{L_1}{\left\|\underline{k}_1\right\|^2} + Bb_{2km}M^{22}\frac{L_2}{\left\|\underline{k}_2\right\|^2}\right)$ (A5)

i and *j* are the indexes of the direction (*i*=1 to 3)and of the node in the element (*j*=1 to 3). *ncelle* is the number of unit cell in the element. The components of the strain interpolation B_{1ij} and B_{2ij} are constant because of the linear interpolation. They are given in Table A1. The in-plane shear interpolation $B_{\gamma ij}$ is:

$$B_{\gamma ij} = B_{1ij}\frac{\underline{k}^1}{\left\|\underline{k}_1\right\|}\cdot\frac{\underline{k}^2}{\left\|\underline{k}^2\right\|} + B_{3ij}\frac{\left\|\underline{k}^2\right\|}{\left\|\underline{k}_1\right\|} + B_{4ij}\frac{\left\|\underline{k}^1\right\|}{\left\|\underline{k}_2\right\|} + B_{2ij}\frac{\underline{k}^2}{\left\|\underline{k}_2\right\|}\cdot\frac{\underline{k}^1}{\left\|\underline{k}^1\right\|} \quad \text{(A6)}$$

B_{3ij} and B_{4ij} are given in Table A1.

The curvatures ate given in function of the position of the nodes of the element and its neighbors.

$$\delta\chi_{\alpha\alpha} = Bb_{\alpha km}\delta u_{km} \quad \text{(A7)}$$

The details of the calculations of the curvature interpolation are given in [41].

Table A1: Membrane strain interpolation components. a and b are the lengths of the element in warp and weft directions

$B_{1i1} = (a-1)k_{1i}$	$B_{1i2} = k_{1i}$	$B_{1i3} = -ak_{1i}$
$B_{2i1} = (b-1)k_{2i}$	$B_{2i2} = -bk_{2i}$	$B_{2i3} = k_{2i}$
$B_{3i1} = (b-1)k_{1i}$	$B_{3i2} = -bk_{1i}$	$B_{3i3} = k_{1i}$
$B_{4i1} = (a-1)k_{2i}$	$B_{4i2} = k_{2i}$	$B_{4i3} = -ak_{2i}$

References

[1] Ruiz E, Trochu F. 19 - Flow modeling in composite reinforcements. In: Boisse P, editor.

Composite Reinforcements for Optimum Performance, Woodhead Publishing; 2011, p. 588–615.
[2] Park CH, Lebel A, Saouab A, Bréard J, Lee WI. Modeling and simulation of voids and saturation in liquid composite molding processes. Composites Part A: Applied Science and Manufacturing 2011;42:658–68.
[3] Deléglise M, Le Grognec P, Binetruy C, Krawczak P, Claude B. Modeling of high speed RTM injection with highly reactive resin with on-line mixing. Composites Part A: Applied Science and Manufacturing 2011;42:1390–7.
[4] Sozer EM, Simacek P, Advani SG. 9 - Resin transfer molding (RTM) in polymer matrix composites. In: Advani SG, Hsiao K-T, editors. Manufacturing Techniques for Polymer Matrix Composites (PMCs), Woodhead Publishing; 2012, p. 245–309.
[5] Blais M, Moulin N, Liotier P-J, Drapier S. Resin infusion-based processes simulation : coupled Stokes-Darcy flows in orthotropic preforms undergoing finite strain. International Journal of Material Forming 2017;10:43–54.
[6] Lukaszewicz DH-JA, Potter KD. The internal structure and conformation of prepreg with respect to reliable automated processing. Composites Part A: Applied Science and Manufacturing 2011;42:283–92.
[7] Khan MA, Reynolds N, Williams G, Kendall KN. Processing of thermoset prepregs for high-volume applications and their numerical analysis using superimposed finite elements. Composite Structures 2015;131:917–26.
[8] Alshahrani H, Hojjati M. Experimental and numerical investigations on formability of out-of-autoclave thermoset prepreg using a double diaphragm process. Composites Part A: Applied Science and Manufacturing 2017;101:199–214.
[9] Verrey J, Wakeman MD, Michaud V, Månson J-AE. Manufacturing cost comparison of thermoplastic and thermoset RTM for an automotive floor pan. Composites Part A: Applied Science and Manufacturing 2006;37:9–22.
[10] Mallick PK. 5 - Thermoplastics and thermoplastic–matrix composites for lightweight automotive structures. In: Mallick PK, editor. Materials, Design and Manufacturing for Lightweight Vehicles, Woodhead Publishing; 2010, p. 174–207.
[11] Guzman-Maldonado E, Hamila N, Boisse P, Bikard J. Thermomechanical analysis, modelling and simulation of the forming of pre-impregnated thermoplastics composites. Composites Part A: Applied Science and Manufacturing 2015;78:211–22.
[12] Henning F, Kärger L, Dörr D, Schirmaier FJ, Seuffert J, Bernath A. Fast processing and continuous simulation of automotive structural composite components. Composites Science and Technology 2019;171:261–79.
[13] Schug A, Rinker D, Hinterhoelzl R, Drechsler K. Evaluating the potential of forming spot-welded layups out of fibre reinforced thermoplastic tape without previous consolidation. International Journal of Material Forming 2019;12:279–93.
[14] Harrison P, Campbell I, Guliyev E, McLelland B, Gomes R, Curado-Correia N, et al. Induction melt thermoforming of advanced multi-axial thermoplastic composite laminates. Journal of Manufacturing Processes 2020;60:673–83.
[15] Danckert J. Experimental investigation of a square-cup deep-drawing process. Journal of Materials Processing Technology 1995;50:375–84.
[16] Wang X, Li J, Deng L, Li J. Metal flow control during hot forming of square cups with local-thickened plates and varied friction conditions. Journal of Materials Processing Technology 2018;253:195–203.
[17] Cherouat A, Billoët JL. Mechanical and numerical modelling of composite manufacturing processes deep-drawing and laying-up of thin pre-impregnated woven fabrics. Journal of Materials Processing Technology 2001;118:460–71.
[18] Cao J, Xue P, Peng X, Krishnan N. An approach in modeling the temperature effect in thermo-stamping of woven composites. Composite Structures 2003;61:413–20.
[19] ten Thije RHW, Akkerman R. A multi-layer triangular membrane finite element for the forming simulation of laminated composites. Composites Part A: Applied Science and Manufacturing 2009;40:739–53.
[20] Peng X, Ding F. Validation of a non-orthogonal constitutive model for woven composite fabrics via hemispherical stamping simulation. Composites Part A: Applied Science and Manufacturing

2011;42:400–7.
[21] Khan MA, Saleem W, Asad M, Ijaz H. A parametric sensitivity study on preforming simulations of woven composites using a hypoelastic computational model. Journal of Reinforced Plastics and Composites 2016;35:243–57.
[22] Aridhi A, Arfaoui M, Mabrouki T, Naouar N, Denis Y, Zarroug M, et al. Textile composite structural analysis taking into account the forming process. Composites Part B: Engineering 2019;166:773–84.
[23] Yu W-R, Harrison P, Long A. Finite element forming simulation for non-crimp fabrics using a non-orthogonal constitutive equation. Composites Part A: Applied Science and Manufacturing 2005;36:1079–93.
[24] Duhovic M, Mitschang P, Bhattacharyya D. Modelling approach for the prediction of stitch influence during woven fabric draping. Composites Part A: Applied Science and Manufacturing 2011;42:968–78.
[25] Bardl G, Nocke A, Hübner M, Gereke T, Pooch M, Schulze M, et al. Analysis of the 3D draping behavior of carbon fiber non-crimp fabrics with eddy current technique. Composites Part B: Engineering 2018;132:49–60.
[26] Liu K, Zhang B, Xu X, Ye J. Experimental characterization and analysis of fiber orientations in hemispherical thermostamping for unidirectional thermoplastic composites. International Journal of Material Forming 2019;12:97–111.
[27] Rashidi A, Milani AS. Passive control of wrinkles in woven fabric preforms using a geometrical modification of blank holders. Composites Part A: Applied Science and Manufacturing 2018;105:300–9.
[28] Lee W, Cao J. Numerical simulations on double-dome forming of woven composites using the coupled non-orthogonal constitutive model. International Journal of Material Forming 2009;2:145.
[29] Khan MA, Mabrouki T, Vidal-Sallé E, Boisse P. Numerical and experimental analyses of woven composite reinforcement forming using a hypoelastic behaviour. Application to the double dome benchmark. Journal of Materials Processing Technology 2010;210:378–88.
[30] Peng X, Rehman ZU. Textile composite double dome stamping simulation using a non-orthogonal constitutive model. Composites Science and Technology 2011;71:1075–81.

[31] Harrison P, Gomes R, Curado-Correia N. Press forming a 0/90 cross-ply advanced thermoplastic composite using the double-dome benchmark geometry. Composites Part A: Applied Science and Manufacturing 2013;54:56–69.
[32] Chen S, Harper LT, Endruweit A, Warrior NA. Formability optimisation of fabric preforms by controlling material draw-in through in-plane constraints. Composites Part A: Applied Science and Manufacturing 2015;76:10–9.
[33] Allaoui S, Boisse P, Chatel S, Hamila N, Hivet G, Soulat D, et al. Experimental and numerical analyses of textile reinforcement forming of a tetrahedral shape. Composites Part A: Applied Science and Manufacturing 2011;42:612–22.
[34] Allaoui S, Hivet G, Soulat D, Wendling A, Ouagne P, Chatel S. Experimental preforming of highly double curved shapes with a case corner using an interlock reinforcement. International Journal of Material Forming 2014;7:155–65.
[35] Mathieu S, Hamila N, Bouillon F, Boisse P. Enhanced modeling of 3D composite preform deformations taking into account local fiber bending stiffness. Composites Science and Technology 2015;117:322–33.
[36] Thompson AJ, Belnoue JP-H, Hallett SR. Modelling defect formation in textiles during the double diaphragm forming process. Composites Part B: Engineering 2020;202:108357.
[37] Wang P, Legrand X, Boisse P, Hamila N, Soulat D. Experimental and numerical analyses of manufacturing process of a composite square box part: Comparison between textile reinforcement forming and surface 3D weaving. Composites Part B: Engineering 2015;78:26–34.
[38] Nishi M, Taketa I, Iwata A, Hirashima T. Constitutive Modeling Of Carbon Fiber Fabric: From Material Parameter Identification To Application In Fe Forming Simulation. 17th European Conference on Composite Materials, 2016.
[39] Bae D, Kim S, Lee W, Yi JW, Um MK, Seong DG. Experimental and Numerical Studies on Fiber

Deformation and Formability in Thermoforming Process Using a Fast-Cure Carbon Prepreg: Effect of Stacking Sequence and Mold Geometry. Materials 2018;11:857.
[40] Zouari B, Daniel J-L, Boisse P. A woven reinforcement forming simulation method. Influence of the shear stiffness. Computers & Structures 2006;84:351–63.
[41] Hamila N, Boisse P, Sabourin F, Brunet M. A semi-discrete shell finite element for textile composite reinforcement forming simulation. International Journal for Numerical Methods in Engineering 2009;79:1443–66.
[42] Launay J, Hivet G, Duong AV, Boisse P. Experimental analysis of the influence of tensions on in plane shear behaviour of woven composite reinforcements. Composites Science and Technology 2008;68:506–15.
[43] Nosrat-Nezami F, Gereke T, Eberdt C, Cherif C. Characterisation of the shear–tension coupling of carbon-fibre fabric under controlled membrane tensions for precise simulative predictions of industrial preforming processes. Composites Part A: Applied Science and Manufacturing 2014;67:131–9.
[44] Mitchell C, Dangora L, Bielmeier C, Sherwood J. Investigation into the changes in bending stiffness of a textile reinforced composite due to in-plane fabric shear: Part 2 – Numerical analysis. Composites Part A: Applied Science and Manufacturing 2016;85:138–47.
[45] Yao Y, Peng X, Gong Y. Influence of tension–shear coupling on draping of plain weave fabrics. Journal of Material Science 2019;54:6310–22.
[46] Alshahrani H. Characterization and finite element modeling of coupled properties during polymer composites forming processes. Mechanics of Materials 2020;144:103370.
[47] Dong L, Lekakou C, Bader MG. Processing of Composites: Simulations of the Draping of Fabrics with Updated Material Behaviour Law. Journal of Composite Materials 2001;35:138–63.
[48] Lin H, Wang J, Long AC, Clifford MJ, Harrison P. Predictive modelling for optimization of textile composite forming. Composites Science and Technology 2007;67:3242–52.
[49] Skordos AA, Monroy Aceves C, Sutcliffe MPF. A simplified rate dependent model of forming and wrinkling of pre-impregnated woven composites. Composites Part A: Applied Science and Manufacturing 2007;38:1318–30.
[50] Boisse P, Hamila N, Vidal-Sallé E, Dumont F. Simulation of wrinkling during textile composite reinforcement forming. Influence of tensile, in-plane shear and bending stiffnesses. Composites Science and Technology 2011;71:683–92.

[51] Hallander P, Akermo M, Mattei C, Petersson M, Nyman T. An experimental study of mechanisms behind wrinkle development during forming of composite laminates. Composites Part A: Applied Science and Manufacturing 2013;50:54–64.
[52] Haanappel SP, ten Thije RHW, Sachs U, Rietman B, Akkerman R. Formability analyses of uni-directional and textile reinforced thermoplastics. Composites Part A: Applied Science and Manufacturing 2014;56:80–92.
[53] Dangora LM, Mitchell CJ, Sherwood JA. Predictive model for the detection of out-of-plane defects formed during textile-composite manufacture. Composites Part A: Applied Science and Manufacturing 2015;78:102–12.
[54] Boisse P, Colmars J, Hamila N, Naouar N, Steer Q. Bending and wrinkling of composite fiber preforms and prepregs. A review and new developments in the draping simulations. Composites Part B: Engineering 2018;141:234–49.
[55] Turk MA, Vermes B, Thompson AJ, Belnoue JP-H, Hallett SR, Ivanov DS. Mitigating forming defects by local modification of dry preforms. Composites Part A: Applied Science and Manufacturing 2020;128:105643.
[56] Latil P, Orgéas L, Geindreau C, Dumont PJJ, Rolland du Roscoat S. Towards the 3D in situ characterisation of deformation micro-mechanisms within a compressed bundle of fibres. Composites Science and Technology 2011;71:480–8.
[57] Belnoue JP-H, Nixon-Pearson OJ, Thompson AJ, Ivanov DS, Potter KD, Hallett SR. Consolidation-Driven Defect Generation in Thick Composite Parts. Journal of Manufacturing Science and Engineering 2018;140.
[58] Wijaya W, Kelly PA, Bickerton S. A novel methodology to construct periodic multi-layer 2D woven unit cells with random nesting configurations directly from μCT-scans. Composites

Science and Technology 2020;193:108125.
[59] Xiong H, Hamila N, Boisse P. Consolidation Modeling during Thermoforming of Thermoplastic Composite Prepregs. Materials 2019;12:2853.
[60] Schäfer, Bastian; Dörr, Dominik; Kärger,Luise, Potential and Challenges of a Solid-Shell Element for the Macroscopic Forming Simulation of Engineering Textiles, Proceedings Esaform 2021.
[61] Lebrun G, Bureau MN, Denault J. Evaluation of bias-extension and picture-frame test methods for the measurement of intraply shear properties of PP/glass commingled fabrics. Composite Structures 2003;61:341–52.
[62] Sharma SB, Sutcliffe MPF, Chang SH. Characterisation of material properties for draping of dry woven composite material. Composites Part A: Applied Science and Manufacturing 2003;34:1167–75.
[63] Lomov SV, Verpoest I. Model of shear of woven fabric and parametric description of shear resistance of glass woven reinforcements. Composites Science and Technology 2006;66:919–33.
[64] Launay J, Hivet G, Duong AV, Boisse P. Experimental analysis of the influence of tensions on in plane shear behaviour of woven composite reinforcements. Composites Science and Technology 2008;68:506–15.
[65] Cao J, Akkerman R, Boisse P, Chen J, Cheng HS, de Graaf EF, et al. Characterization of mechanical behavior of woven fabrics: Experimental methods and benchmark results. Composites Part A: Applied Science and Manufacturing 2008;39:1037–53.
[66] Zhu B, Yu TX, Teng J, Tao XM. Theoretical Modeling of Large Shear Deformation and Wrinkling of Plain Woven Composite. Journal of Composite Materials 2009;43:125–38.
[67] Boisse P, Hamila N, Guzman-Maldonado E, Madeo A, Hivet G, dell'Isola F. The bias-extension test for the analysis of in-plane shear properties of textile composite reinforcements and prepregs: a review. International Journal of Material Forming 2017;10:473–92.
[68] Hosseini A, Kashani MH, Sassani F, Milani AS, Ko FK. Identifying the distinct shear wrinkling behavior of woven composite preforms under bias extension and picture frame tests. Composite Structures 2018;185:764–73.
[69] F. T. Peirce B.Sc. FTI FInstP. 26—the "Handle" of Cloth as a Measurable Quantity. Journal of the Textile Institute Transactions 1930;21:T377–416.

[70] ASTM E. 1130–02: Standard test method for objective measurement of speech privacy in open offices using articulation index. Am. Soc. for Testing and Materials. Philadelphia. USA; 2002.
[71] de Bilbao E, Soulat D, Hivet G, Gasser A. Experimental Study of Bending Behaviour of Reinforcements. Experimental Mechanics 2010;50:333–51.
[72] Mallach A, Härtel F, Heieck F, Fuhr J-P, Middendorf P, Gude M. Experimental comparison of a macroscopic draping simulation for dry non-crimp fabric preforming on a complex geometry by means of optical measurement. Journal of Composite Materials 2017;51:2363–75.
[73] Wang J, Long AC, Clifford MJ. Experimental measurement and predictive modelling of bending behaviour for viscous unidirectional composite materials. International Journal of Material Forming 2010;3:1253–66.
[74] Sachs U, Akkerman R. Viscoelastic bending model for continuous fiber-reinforced thermoplastic composites in melt. Composites Part A: Applied Science and Manufacturing 2017;100:333–41.
[75] Dörr D, Schirmaier FJ, Henning F, Kärger L. A viscoelastic approach for modeling bending behavior in finite element forming simulation of continuously fiber reinforced composites. Composites Part A: Applied Science and Manufacturing 2017;94:113–23.
[76] Alshahrani H, Hojjati M. A theoretical model with experimental verification for bending stiffness of thermosetting prepreg during forming process. Composite Structures 2017;166:136–45.
[77] Kawabata S, Niwa M, Kawai H. 3—the Finite-Deformation Theory of Plain-Weave Fabrics Part I: The Biaxial-Deformation Theory. The Journal of The Textile Institute 1973;64:21–46.
[78] Buet-Gautier K, Boisse P. Experimental analysis and modeling of biaxial mechanical behavior of woven composite reinforcements. Experimental Mechanics 2001;41:260–9.
[79] Willems A, Lomov SV, Verpoest I, Vandepitte D. Optical strain fields in shear and tensile testing of textile reinforcements. Composites Science and Technology 2008;68:807–19.
[80] Carvelli V, Corazza C, Poggi C. Mechanical modelling of monofilament technical textiles.

Computational Materials Science 2008;42:679–91.
[81] Adumitroaie A, Barbero EJ. Beyond plain weave fabrics – I. Geometrical model. Composite Structures 2011;93:1424–32.
[82] Prodromou AG, Chen J. On the relationship between shear angle and wrinkling of textile composite preforms. Composites Part A: Applied Science and Manufacturing 1997;28:491–503.
[83] Rozant O, Bourban P-E, Månson J-AE. Drapability of dry textile fabrics for stampable thermoplastic preforms. Composites Part A: Applied Science and Manufacturing 2000;31:1167–77.
[84] Hübner M, Diestel O, Sennewald C, Gereke T, Cherif C. Simulation of the Drapability of Textile Semi-Finished Products with Gradient-Drapability Characteristics by Varying the Fabric Weave. Fibres & Textiles in Eastern Europe 2012:88--93.
[85] Oñate E, Zárate F. Rotation-free triangular plate and shell elements. International Journal for Numerical Methods in Engineering 2000;47:557–603.
[86] Pazmino J, Carvelli V, Lomov SV. Formability of a non-crimp 3D orthogonal weave E-glass composite reinforcement. Composites Part A: Applied Science and Manufacturing 2014;61:76–83.
[87] Pazmino J, Mathieu S, Carvelli V, Boisse P, Lomov SV. Numerical modelling of forming of a non-crimp 3D orthogonal weave E-glass composite reinforcement. Composites Part A: Applied Science and Manufacturing 2015;72:207–18.
[88] de Luca P, Lefébure P, Pickett AK. Numerical and experimental investigation of some press forming parameters of two fibre reinforced thermoplastics: APC2-AS4 and PEI-CETEX. Composites Part A: Applied Science and Manufacturing 1998;29:101–10.
[89] Vanclooster K, Lomov SV, Verpoest I. On the formability of multi-layered fabric composites. Proc 17th Int Conf Compos Mater, 2009, p. 1–10.
[90] Guzman-Maldonado E, Wang P, Hamila N, Boisse P. Experimental and numerical analysis of wrinkling during forming of multi-layered textile composites. Composite Structures 2019;208:213–23.
[91] Liu L, Zhang T, Wang P, Legrand X, Soulat D. Influence of the tufting yarns on formability of tufted 3-Dimensional composite reinforcement. Composites Part A: Applied Science and Manufacturing 2015;78:403–11.